nature nanotechnology

SUPPLEMENTARY INFORMATION

DOI: 10.1038/NNANO.2017.24

In the format provided by the authors and unedited.

Quantized edge modes in atomic-scale point contacts in graphene

Amogh Kinikar, T. Phanindra Sai, Semonti Bhattacharyya, Adhip Agarwala, Tathagata Biswas, Sanjoy K. Sarker, H. R. Krishnamurthy, Manish Jain, Vijay B. Shenoy and Arindam Ghosh

Supplementary Information contents:

1 Experimental insight into nanoexfoliation process

Ultraclean single/few layer graphene flakes were exfoliated from highly oriented pyrolitic graphite (HOPG) substrate with a metallic tip in a highly controlled operation. To achieve capability of *in situ* electrical measurement and simultaneous high resolution imaging we have modified the sample mounting stage in the scanning electron microscope (Sigma, Zeiss, UK). A picture of the experimental setup is shown in Fig. S1(a). The compact metallic enclosure designed to house the piezo and attocube system for low temperature and high magnetic field measurement is shown in Fig. S1(b). Considerable care was taken to isolate this compact enclosure from mechanical vibrations by suspending it with springs. In addition the low temperature cryostat was mounted in a dewar placed on a vibration isolation system consisting of sand, heavy granite slabs, rubber isolator composite structure.

During the in-situ measurements in SEM, coarse positioning of graphite crystal near to the tip was performed by using the attocube system while the motion of graphite crystal was observed with the SEM. The final approach was performed with a piezo-electric tube. The piezo voltage was varied in the range of -200 V to + 200 V at different rates from $3 - 1500$ V/min ($0.18 - 90$ μm/min) during approach and retreat operation. To understand the process of exfoliation, SEM images were obtained at different stages of approach and retreat processes. Fig. S2(a) shows the SEM images obtained during a typical approach. In Fig. S2(b) the SEM images obtained during the corresponding retreat operation are shown, where the tapering of exfoliate can be clearly seen from the track marks left by the exfoliate on the graphite crystal surface. Simultaneous electrical measurements were carried out only on few exfoliations as it has been observed that the exposure to high dose of electron beam introduces large series resistance most likely due to the structural damage to the exfoliates as described in the methods section. During most of the exfoliations it was observed that invariably large chunk of graphite flakes stick to tip indicating that tapering and rupture occur near the graphite crystal surface or far away from the tip. In Fig. S2(c) false colored SEM images of the pristine tip (panel 1) and images obtained during the subsequent retreat operation (panel 2,3,4) are shown. It can be clearly seen from the image in panel 4 that a large

chunk of graphite present on the tip. This rules out the possibility of quantization effects observed in the electrical measurements, being caused by formation of point contact at the tip graphene interface. In Fig. S2(d) SEM images of the flakes present on the tip after a exfoliation process are shown, where a tapering of 60° and 30° can be seen. During exfoliation process graphene flakes showed appreciable intensity contrast with background graphite crystal substrate during SEM imaging. From the image analysis, which is described in the caption of Fig. S3 it can be concluded that the exfoliated flakes just before rupture mostly consist of one to two layers of graphene.

To obtain a better understanding of the rupture process and to determine the thickness of the flakes close to rupture (< 20 nm from the point of rupture) AFM (atomic force microscope) imaging was used. AFM imaging was done at exfoliation sites created during exfoliation of the graphite crystal surface by the metallic tip. Over 50 such exfoliation sites were scanned and it was found that close to final rupture, 32% exfoliations are single layered graphene with 30° tapering angle, such as shown in Fig. 1(b) and Fig. S4(a). About 21% exfoliations had 60° tapering angle, mostly at bilayer thickness, such as shown in Fig. S4(b). The histogram of depth (equivalent to the thickness of the exfoliate) obtained from the line profiles taken < 20 nm from the apex (rupture point) is shown in Fig. S4(c) upper panel. The histogram of tapering angle obtained < 20 nm from the apex (rupture point) is shown in Fig. S4(c) lower panel. It can be concluded from the AFM analysis confirms high-symmetry tapering of the exfoliates down to single layer graphene thickness.

Our exfoliations were mostly carried out in vacuum, except a few cases of deliberate exfoliations in ambiance or inert argon atmosphere. As shown in Fig. 1c, the details of the environment during exfoliation does not have a discernible impact on the quantitative features of the observed conductance states. Thus a chemical contamination can essentially be ruled out, even when the exfoliation is carried out in the ambient condition. This somewhat non-intuitive observation can be understood with a simple estimation of the time scale (t_b) for a gas molecule to bind at a ZZ edge dangling bond. Roughly, the rate at which a gas molecule can bind at the edge can be written as,

t_b^{-1}=$P \times t_{act}^{-1}$, where P is the probability of finding a gas molecule within a distance of the dangling bond size ($\sim 1\mathring{A}$), and t_{act}=t_0 exp(ΔE/k$_B$T) $\approx 10^3 - 10^4$ seconds, is time to bind to the dangling bond by overcoming the activation energy barrier ΔE $\sim$ 1 eV. Since the electrically relevant region of the (ZZ) edge extends only about $10 - 20$ nm from the point of final rupture (see discussion in connection with Fig. 3), we find P $\sim$ 0.01, even at ambient pressure and temperature. Thus with the method of fast exfoliation, the exfoliation time scale ($\sim$ 3 seconds) is nearly six to seven orders of magnitude shorter than the time scale of the gas molecule-based contamination.

2 Computational Details

In order to understand the role of electron-electron interaction on the electronic structure of the nanoconstriction, we studied the low energy Hubbard Hamiltonian of this constriction. The Hubbard Hamiltonian for this system can be written as:

$$\mathcal{H} = \sum_{\langle ij \rangle \sigma} -t c_{i,\sigma}^{\dagger} c_{j,\sigma} + h.c. + \sum_{i} U \hat{n}_{i,\uparrow} \hat{n}_{i,\downarrow} \tag{1}$$

where $c_{i,\sigma}^{\dagger}$ ($c_{i,\sigma}$) is the creation (annihilation) operator to create (annihilate) an electron with spin σ at site i, t is the nearest-neighbor hopping energy (= 2.7 eV), U is the onsite Coulomb repulsion, $\hat{n}_{i,\uparrow}$ and $\hat{n}_{i,\downarrow}$ are the up and down charge density at site i. This low energy Hamiltonian can be used to describe the π bonding network in graphene. The onsite Coulomb energy, U has been reported to have values ranging from $0.5 - 2.0t$ and is strongly influenced by the screening from the substrate. Within the mean-field approximation, one can simplify the above Hamiltonian as:

$$\mathcal{H}_{MFT} = \sum_{\langle ij \rangle \sigma} -t c_{i,\sigma}^{\dagger} c_{j,\sigma} + h.c. + \sum_{i,\sigma} U \hat{n}_{i,\sigma} \langle \hat{n}_{i,\bar{\sigma}} \rangle - \sum_{i} U \langle \hat{n}_{i,\downarrow} \rangle \langle \hat{n}_{i,\uparrow} \rangle \tag{2}$$

We self-consistently solved the Hubbard Hamiltonian within mean-field approximation (for various values of U) for the system shown in Fig. S8a containing 4914 lattice sites. In order to determine the magnetic ordering in this nanoconstriction, we started from both the ferromagnetic as well as anti-ferromagnetic initial configurations. In the anti-ferromagnetic configuration the A and B sub-lattice sites have opposing moments, while in the ferromagnetic configuration they

have moments in the same direction. We found that the anti-ferromagnetically ordered state is always lower in energy than the ferromagnetically ordered one. This magnetic ordering is similar to magnetic ordering in graphene nanoribbons with zig-zag edges. In those nanoribbons, each edge orders in the same fashion with anti-ferromagnetic ordering between the edges. In this nanoconstriction, we have only one zig-zag edge (leading to only one edge state). The ordering of this edge is in that sense similar to one of the graphene nanoribbon edges. The calculated spin resolved density-of-states for different values of effective electron-electron interaction (U/t) are shown in Fig. S8b.

3 Theoretical modeling for the torn graphene

In this section we mention briefly the motivation and the details of our theoretical model in order to understand the experimental results. The conductance traces (see Fig.1c) can be understood as arising from the nature of initial contact of the tip and subsequent fracture of the exfoliations from the graphite crystal surface. The initial state can be such that there are a large number of fragments bridging the tip and graphite crystal. Smoother variations (without quantized steps) can thus arise from the myriad of bridging nanostructures that continually snap with increasing retraction distance. Sharp plateaus occur when a few large ribbons bridge across.

Further to understand the sub-G_0 conductances we model a 30° torn GNR via an effective tight binding description and perform Non-Equilibrium Green's Function(NEGF) [1,2] calculations. A 30° tear in graphene nanoribbon occurs when one of the edges remains a zig-zag while the other tears as an arm-chair edge. The geometry of the ribbons is defined by the number of graphene hexagons (N_{L} and N_{C})which constitute the width at the broader and narrower side, called in this work, as W_{L} and W_{C} respectively ($N_{\mathrm{L,C}}$ = $W_{\mathrm{L,C}}$ / 0.24(nm)). Next we consider only nearest neighbor hopping with the hopping integral $t \sim 2.7$ eV [3]. Now for completeness we mention the essential methodology of the NEGF calculations [1,2].

Essentially a two terminal conductance experiment comprises of two leads and an intermedi-

ate device. An evaluation of the total transmission of the same, $T(E)$ at a particular energy E, can be related to the conductance by $G = \frac{2e^2}{h}T(E)$. While the device is a finite size mesoscopic system and is described by a Hamiltonian matrix H_D, the leads are modeled by infinitely large systems of a repeating unit cell. The prescription is to evaluate the self energies of the right and left lead, $\Sigma_R(E)$ and $\Sigma_L(E)$ and then evaluate the coupling matrices $\Gamma_{R(L)}(E)$ given by $= i(\Sigma_{R(L)}(E) - \Sigma^{\dagger}_{R(L)}(E))$. The Green's function of the device is now given by $G_D(E) = [E - H_D - \Sigma_L(E) - \Sigma_R(E)]^{-1}$. The total transmission can be then evaluated using,

$$T(E) = Tr[\Gamma_L(E)G^{\dagger}_D(E)\Gamma_R(E)G_D(E)] \tag{3}$$

In our calculations the 30° tear region as shown in Fig. S10a is considered to be the device part. The leads are assumed to be infinite zig-zag ribbons of widths corresponding to W_{L} and $W_{textscc}$ coupled with the central device on the corresponding broader and narrower sides respectively. Note that in this configuration one of the zig-zag edges remains uninterrupted over the whole system. The calculations were performed at $E/t \sim 0.031$ (~ 0.08 eV) for graphite crystal sample. The tear experiment close to the final snapping of the contact can be understood as a sequential decrease in W_{C} for a fixed W_{L}.

In the Fig. S10b we show the results for values of N_{L} from $6 - 43$ which corresponds to the broader width of $\sim$ 1-10 nm and then sequentially decrease the value of N_{C} for each N_{L}. One can notice clustering of the conductance values close to nearly some rational fractions. An understanding of this problem from the perspective of a Dirac theory could be an interesting theory project.

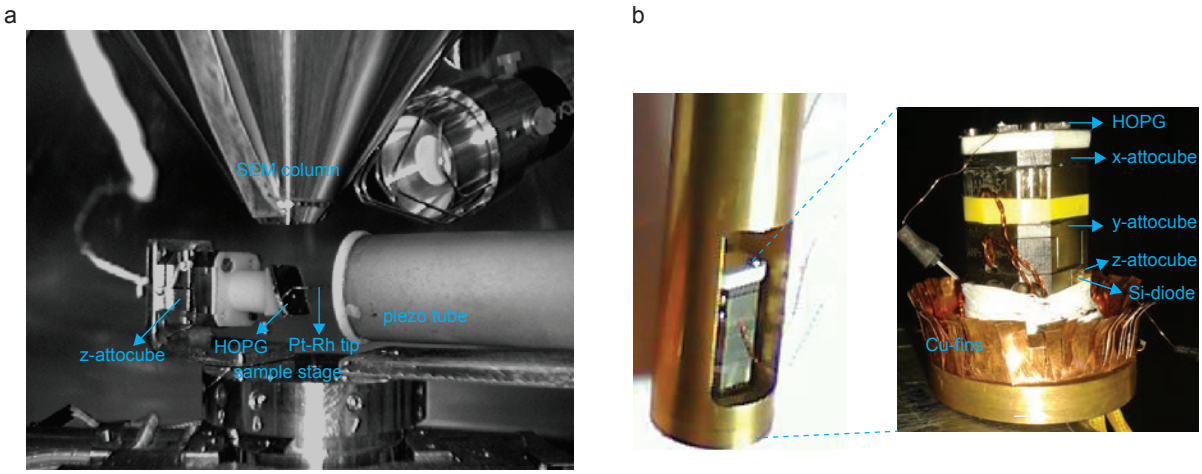

Figure S1: **Photograph of the experimental setup. a,** photograph of the *in situ* exfoliation setup inside SEM. **b,** photograph of the setup designed for in-situ exfoliation at low temperature and high magnetic field measurements.

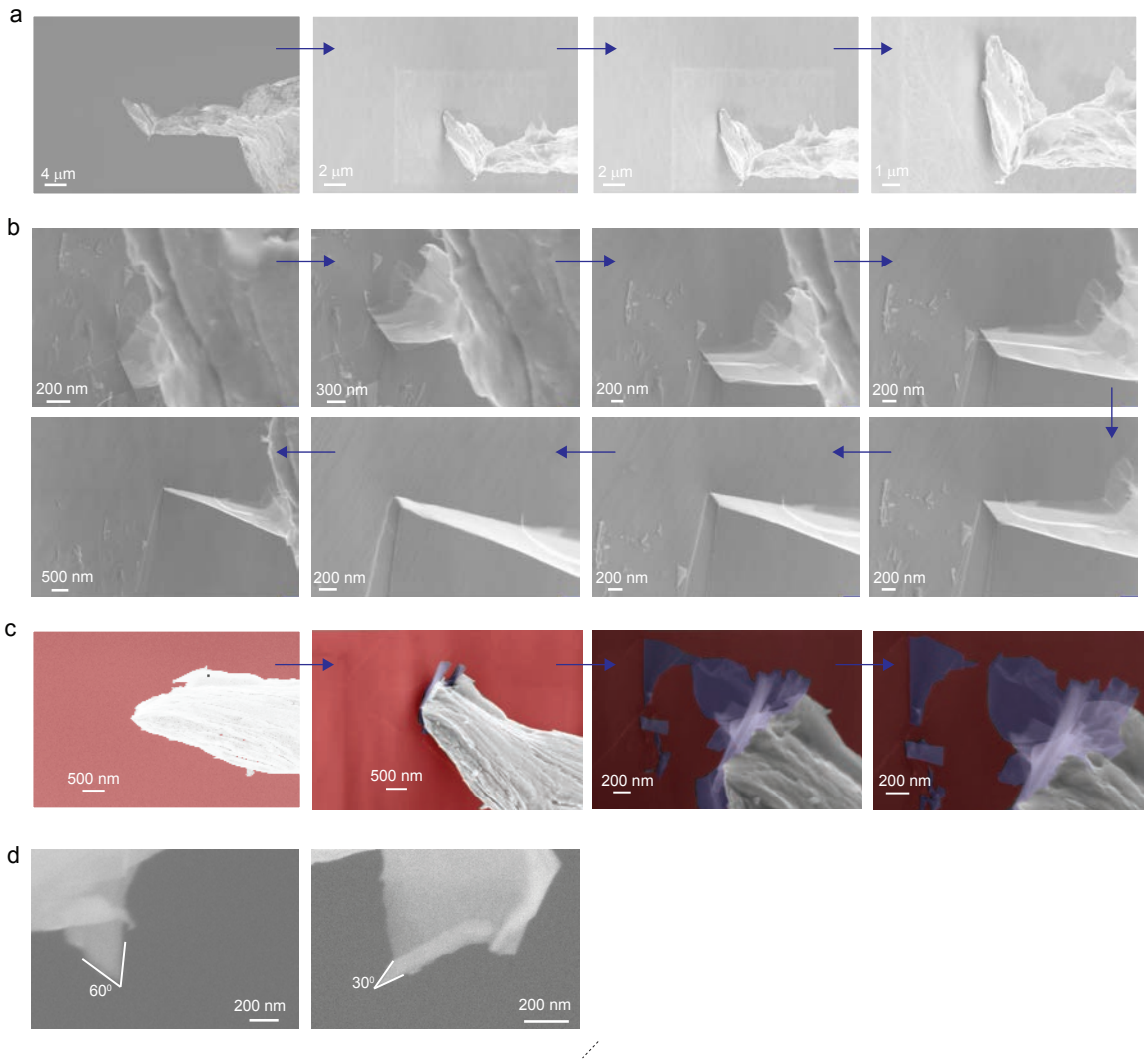

Figure S2: **SEM images of approach and retreat process. a,b** sequence (time sequence indicated by arrow direction) of SEM images obtained during approach and retract process, respectively, of the tip from the graphite crystal, **c,** false colored SEM images of a pristine tip (panel 1) and the sequence obtained during subsequent retreat process (panel 2,3,4). From image in panel 4 it can be observed that the exfoliation causes a bulk chunk of graphitic flake attached on the tip, ruling out formation of point contact at the tip-graphite interface. **d,** post-rupture SEM images of graphitic flakes protruding from tip showing angles of 60°, 30°.

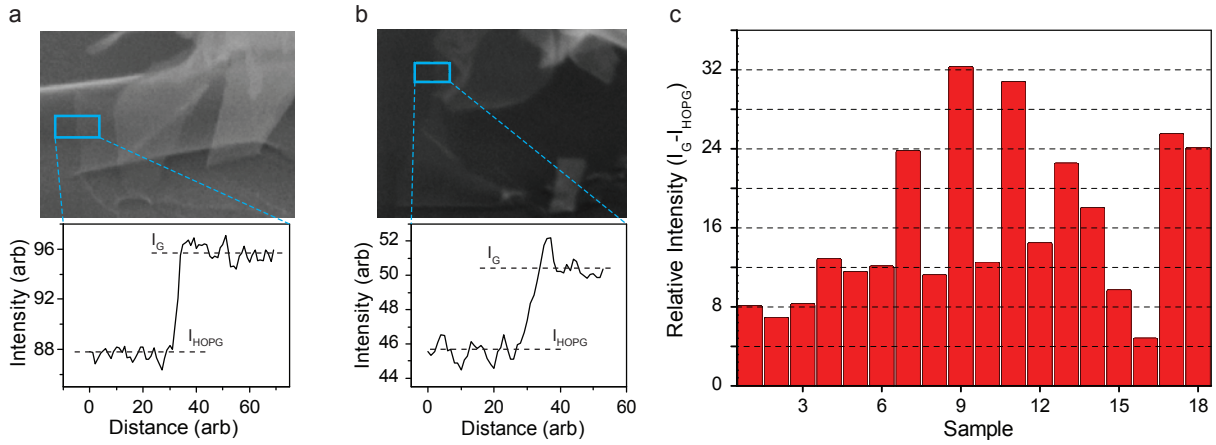

Figure S3: **Estimation of the thickness of exfoliated flakes. a,b,** SEM image obtained for estimation thickness of exfoliates, during a typical retraction process showing intensity variation across the track marks left by the exfoliates on the graphite crystal substrate, as well as the suspended exfoliates forming tapered bridges at the graphite crystal. Since the contrast (of ultra-thin exfoliates against the graphite crystal background) arises due to absorption of secondary electrons emitted from graphite crystal as they travel through the exfoliate, we can assume the contrast ($= I_{\mathrm{G}} - I_{\mathrm{HOPG}}$, where I_{G} and I_{HOPG} are the intensities from exfoliate region and the adjacent graphite crystal regions respectively) to be proportional to the thickness of the exfoliate. (A detailed quantitative analysis of the SEM-based thickness determination of ultra-thin graphene films can be found in [4]). The lower panels show the variation of intensity obtained from highlighted area on SEM image. **c,** relative intensity ($I_{\mathrm{G}} - I_{\mathrm{HOPG}}$) from 18 different exfoliations varies in units of ~ 4, indicating the discrete nature of the thickness variation among the exfoliates. Assuming the lowest contrast to correspond to a single layer graphene, we find most exfoliates to lie between two to four layers. Importantly, the images analyzed here are those from initial stage of exfoliation. At the verge of rupture, the exfoliates would probably consist of one or two layers of graphene as confirmed by the AFM characterization.

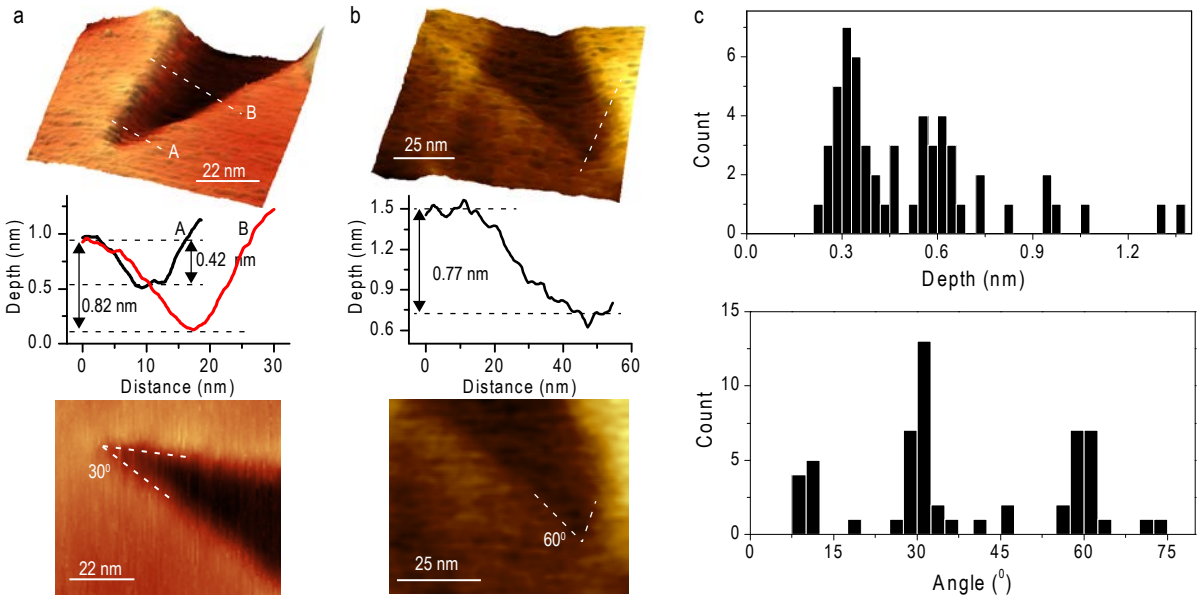

Figure S4: **Post-rupture topography maps and tapering angle statistics. a,b,** AFM topography map at a typical exfoliation site on the graphite crystal surface (upper panel), the line scans show a layer-by-layer structural evolution during the final stage of the exfoliation (central panel), and surface map showing tapering of exfoliation prior to the final rupture at 30° and 60° respectively. **c,** Variation of the depth with tapering angle (< 20 nm from apex) at the final stage of exfoliation (upper panel) and 2D histogram of depth and tapering angle (lower panel), indicating that nearly 60% of the exfoliations are dominated by high symmetry 30° and 60° tapering angle.

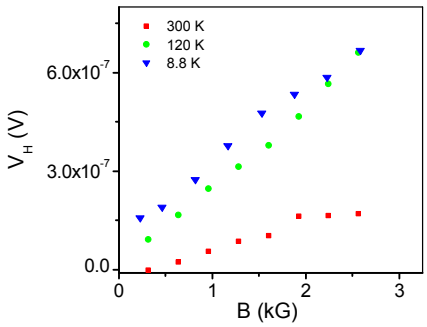

Figure S5: **Hall voltage.** Dependence of Hall voltage (V_{H}) on magnetic field (B) at 8.8 K, 120 K and 300 K measured on the graphite crystal substrate using Van der Pauw method. The measurement yields an areal carrier density of $\sim 2-3\times10^{15}$ m^{-2} at 300 K which reduces to $\sim 10^{15}$ m^{-2} at lower temperatures (120 K and 8.8 K) due to the freezing of carriers. This unintentional doping of graphite crystal shifts the local Fermi energy to $\sim$ 80 meV at 300 K and $\sim$ 30 meV at 9 K. It should, however, be noted that due to the suspended nature of the exfoliates, the local doping of the point contacts, especially at low temperatures can be significantly smaller than the above estimate, and also vary from one region of the graphite crystal surface to the other.

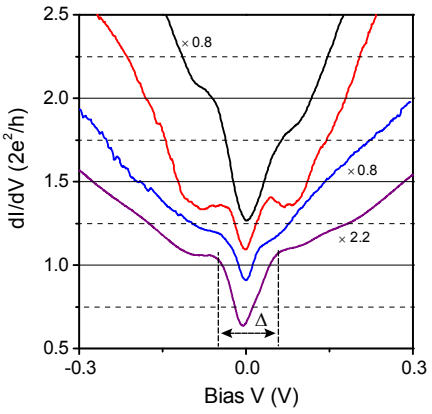

Figure S6: **Differential conductance.** (dI/dV) as a function of voltage (V) between metal tip and graphite crystal substrate, obtained from different exfoliations at similar zero-bias conductance values ($\sim$ 0.5 - 1$\times$G$_0$, the traces are shifted for clarity) at 8.8 K. The double peak structure shows a gap like feature, indicated by Δ, which is remarkably similar among different exfoliations has a modal value $\approx$ 0.1 eV as shown in Fig. 2c.

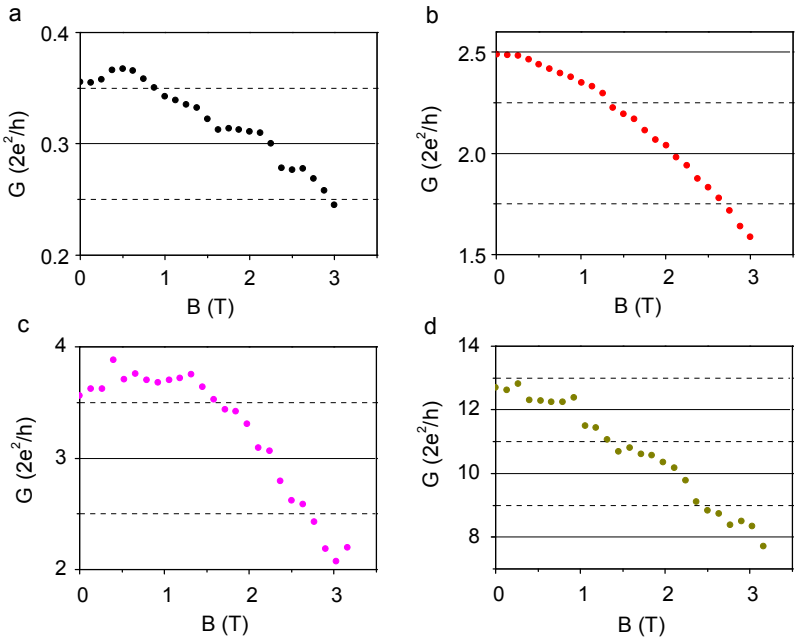

Figure S7: **Magnetic field dependence of zero-bias conductance. a,b,c,d,** zero-bias conductance as function of magnetic field for exfoliations in different conductivity range. The decrease in $G(B)$ for $B \gtrsim 1$ T follows $\ln[G(B)] = -\alpha B^2$ (see Fig. 2h) even for G as high as $12G_0$, which is a consequence of squeezing of evanescent waves in magnetic field. The constant of proportionality $\alpha \approx 0.05$ T^{-2}, which depends on the localization length and distance between the pinning centers, is also remarkably similar for different conductance magnitudes. This strongly suggests localization of the edge states in each tapered exfoliates connecting the metal tip and the graphite crystal. Since each exfoliate is structurally similar, the value of α does not change drastically even when the number of parallel exfoliates (and hence the conductance) is large.

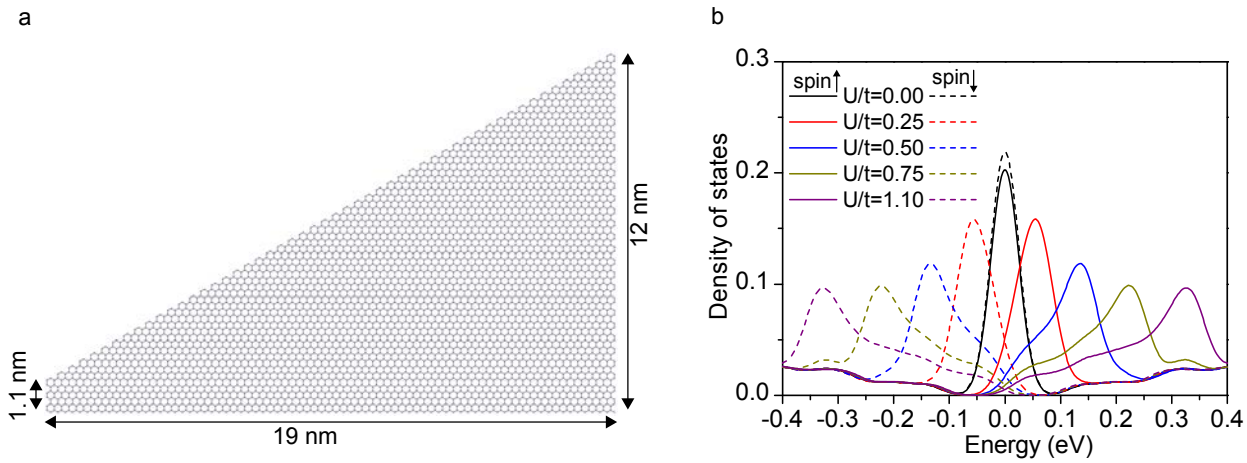

Figure S8: **Computation of spin resolved density-of-states. a,** Model of 30° tapered nanoribbon containing 4914 lattice sites. **b,** Calculated spin resolved density-of-states for the model shown in (**a**) for different values of the effective electron-electron interaction (U/t) (see section 2).

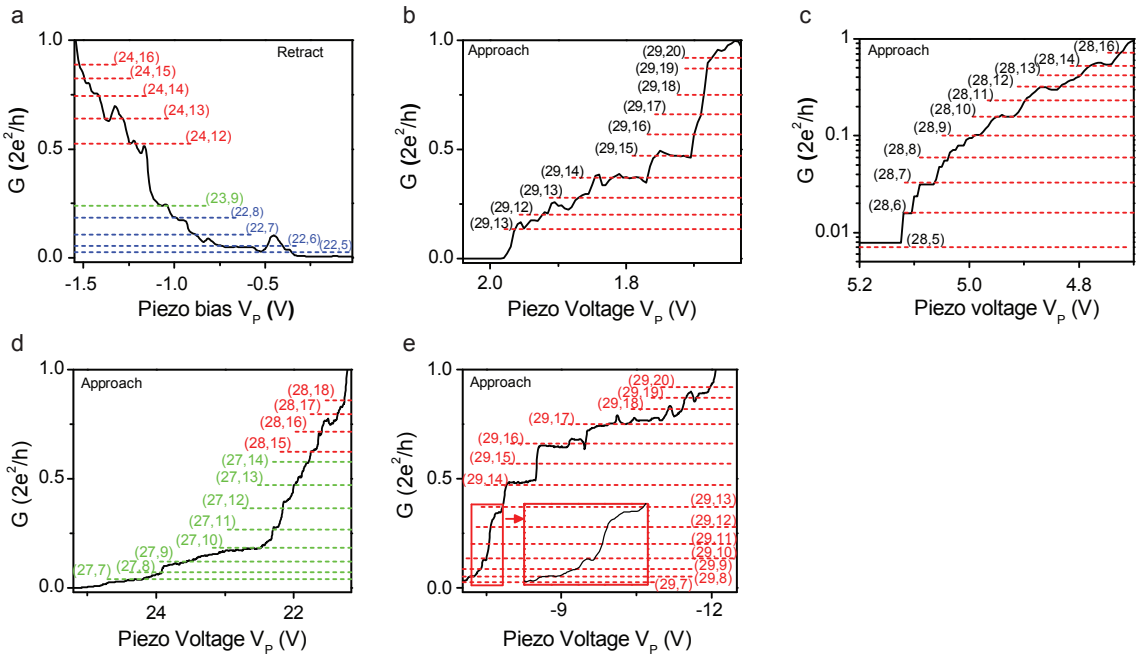

Figure S9: **Fractional conductance. a,b,c,d,e,** fractional conductance data obtained during approach and retract cycles of exfoliation from graphite crystal at 300 K, the dashed lines indicate the theoretical value representing $(N_{\mathrm{L}}, N_{\mathrm{C}})$ (see section 3, Fig. 3 and Fig. S10 for details).

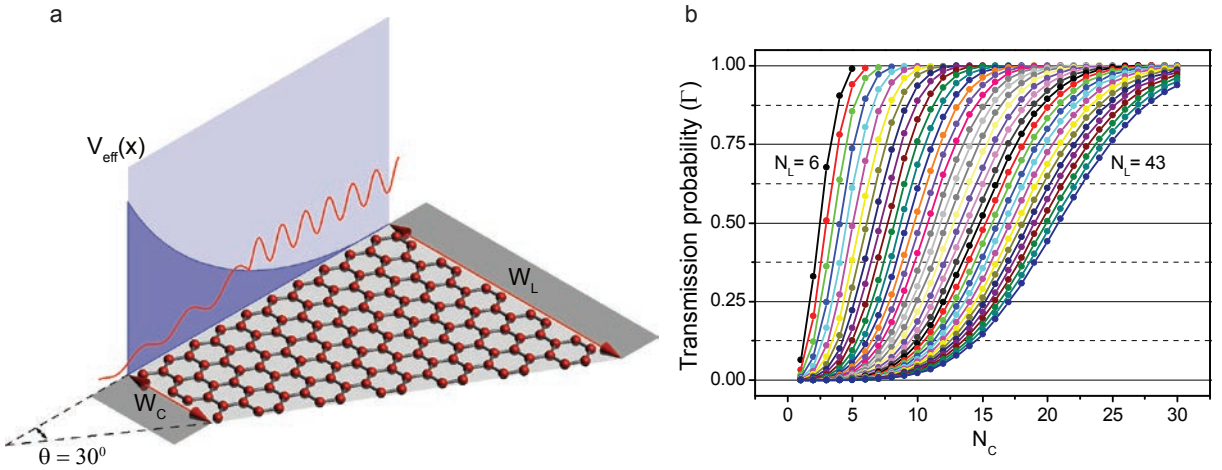

Figure S10: **Theoretical modeling for the torn graphene. a,** A model of a 30° torn graphene nanoribbon terminated by armchair and zigzag edges used in theoretical calculations. N_{L} and N_{C} are the number of carbon hexagons which build up the GNR on the broader and narrower sides respectively. Edge states on the zig-zag edges which are responsible for transport see an effective potential(schematically shown as $\mathrm{V}_{eff}(\mathrm{x})$ due to the narrowing of the ribbon. This potential renders the transmission to be less than unity. **b,** Calculated transmission coefficient as a function of N_{C} using NEGF calculations on the effective tight binding model for the graphite crystal. Different curves are for different values of N_{L} (left most $N_{\mathrm{L}} = 6$ and the right most is for $N_{\mathrm{L}} = 43$).

References

[1] Datta, S. *Electronic transport in mesoscopic systems* (Cambridge university press, 1997).

[2] Muñoz Rojas, F., Jacob, D., Fernández-Rossier, J. & Palacios, J. J. Coherent transport in graphene nanoconstrictions. *Phys. Rev. B* **74**, 195417 (2006).

[3] Reich, S., Maultzsch, J., Thomsen, C. & Ordejón, P. Tight-binding description of graphene. *Phys. Rev. B* **66**, 035412 (2002).

[4] Kochat, V. *et al.* High contrast imaging and thickness determination of graphene with in-column secondary electron microscopy. *J. Appl. Phys.* **110**, 014315 (2011).